



Received July 31, 2024; accepted January 06, 2025; Date of publication February 12, 2025.
The review of this paper was arranged by Associate Editor Margarita Norambuena[✉] and Editor-in-Chief Heverton A. Pereira[✉].

Digital Object Identifier <http://doi.org/10.18618/REP.e202517>

Design Guide for Integral CCS-MPC Applied to a Surface Permanent Magnet Synchronous Motor with HiL Implementation

Arthur G. Bartsch^{✉1,*}, Rodrigo Trentini^{✉1}, Ademir Nied^{✉2}, José de Oliveira^{✉2},
Filipe Fernandes^{✉2}, Sabrina F. dell Agnolo^{✉2}, Mariana S. M. Cavalca^{✉2}

¹Federal Institute of Santa Catarina, Department of Electrical Engineering, Jaraguá do Sul – Santa Catarina, Brazil.

²Santa Catarina State University, Department of Electrical Engineering, Joinville, SC, Brazil.

e-mail: arthur.bartsch@ifsc.edu.br^{*}; rodrigo.trentini@ifsc.edu.br; ademir.nied@udesc.br; jose.oliveira@udesc.br;
filipe02.fernandes@gmail.com; sabrina.dellagnolo@gmail.com; mariana.cavalca@udesc.br

^{*}Corresponding author

ABSTRACT This paper presents a design guide for applying an integral convex control set model-based predictive control (CCS-MPC) in a surface permanent magnet synchronous machine (SPMSM). The proposed CCS-MPC has an intrinsic integral action that eliminates the need of an external disturbance estimator for disturbance rejection. In the control design, this work presents a relation between the open-loop cost function weighting factor and the closed-loop bandwidth factor, which could be used to improve the controller design. Several tests are performed in the hardware-in-the-loop experimental, as sinusoidal and step reference tracking. Experimental frequency responses are also provided.

KEYWORDS CCS-MPC, Integral control, SPMSM.

I. INTRODUCTION

Model-based predictive control (MPC) has been extensively researched in power electronics and motor control applications over the last decade [1]–[5]. The interest in MPC arises from its flexibility and capabilities as a control strategy [6].

There are two main approaches to applying MPC in power electronics, distinguished by how the control action is described. When the control action is limited to a finite set of switch states, it is referred to as Finite Control Set (FCS) MPC. Conversely, if the control action is modulated and considered a real value, it is known as Convex Control Set (CCS) MPC [7].

Both common formulations of MPC face difficulties when integral action is required, especially if the control is not informed about the steady-state control action [8]. Several formulations have been proposed to incorporate integral action in different scenarios.

The standard method for implementing an integrator effect in MPC is to augment the state-space model and redefine the states based on their variations [9]. However, this approach is limited to tracking DC references and is highly sensitive to noise [8].

In the context of motor control, both CCS and FCS-MPC commonly use a load estimator and feedforward control. This estimator can exploit certain properties of the MPC formulation [10] or be a state observer with an augmented model [11]. These methods are designed independently of the control and can influence the designed dynamics.

In other MPC application contexts, a possible solution is to consider previous samples, compare the actual values with the expected steady-state values, and add the difference to the control action [12]. This approach is similar to Dynamic Matrix Control (DMC) [13], but it requires storing past samples and typically works only for DC references. Another solution is to include the accumulated error penalization in the MPC cost function [14]. This makes the MPC formulation more complex and results in a non-zero cost function at the minimum. However, it allows for AC reference tracking and does not depend on an external disturbance estimator, thus preserving the closed-loop response.

Therefore, this paper specifically studies this latter MPC formulation in the context of motor control. This formulation involves a significant number of weighting factors, which complicates the control design and can degrade the closed-loop performance. Additionally, applying this control to a permanent magnet synchronous motor (PMSM) has unique challenges due to the nonlinear nature of the motor model. Hence, this paper presents a design guide for this type of MPC applied to surface PMSM. This work builds on previous studies [5], [15]–[17], and is a direct extension of a paper originally published in the 2023 IEEE 8th Southern Power Electronics Conference and 17th Brazilian Power Electronics Conference (SPEC/COBEP) [18], which is a continuation of the paper published in the 2019 IEEE 5th Southern Power Electronics Conference and 15th Brazilian Power Electronics Conference (SPEC/COBEP) [16]. The novelty of this paper lies in the clear design guide presented,

the detailed results and analysis, and the introduction of a normalization step in the application of this controller. The results of this paper are evaluated using Hardware in the Loop (HiL) with a Typhoon HiL setup.

Section II presents the PMSM modeling. Section III presents the MPC formulation. Section IV presents the proposed design guide. Section V provides an application example of the proposed design guide. Section VI describes the methods used to obtain the results. Section VII presents the results. Finally, Section VIII concludes the work.

II. SURFACE PMSM AND INVERTER MODELING

This section presents the motor and the inverter modeling.

A. Motor model in continuous-time

The PMSM is a continuous nonlinear system. We consider these hypotheses to obtain a mathematical model: saturation and hysteresis can be neglected; Coulumb Friction and cogging torque can be neglected; the motor is symmetrical; the dq transformation can be used to represent the motor. Therefore, in dq -coordinates for electrical variables, the surface PMSM dynamical behavior is given by:

$$\begin{aligned} \dot{\mathbf{x}}(t) &= \mathbf{A}_c(\mathbf{x}(t))\mathbf{x}(t) + \mathbf{B}_c\mathbf{u}(t) + \mathbf{E}_c\mathbf{d}(t) \\ \mathbf{y}(t) &= \mathbf{C}_c\mathbf{x}(t) \end{aligned} \quad (1)$$

whereas

$$\mathbf{x}(t) = [i_{ds}(t) \quad i_{qs}(t) \quad \omega_e(t)]^T, \quad (2)$$

$$\mathbf{u}(t) = [v_{ds}(t) \quad v_{qs}(t)]^T, \quad (3)$$

$$\mathbf{y}(t) = [i_{ds}(t) \quad \omega_e(t)]^T, \quad (4)$$

$$\mathbf{d}(t) = \tau_l(t) \quad (5)$$

being i_{ds} the direct axis current [A], i_{qs} the quadrature axis current [A], v_{ds} the direct axis voltage [V], v_{qs} the quadrature axis voltage [V], ω_e the electrical angular speed [rad/s], τ_l the load torque [Nm], and being

$$\mathbf{A}_c(\mathbf{x}(t)) = \begin{bmatrix} -\frac{R_s}{L_s} & \omega_e(t) & 0 \\ -\omega_e(t) & -\frac{R_s}{L_s} & -\frac{\Lambda_{pm}}{L_s} \\ \frac{3N_p^2\Lambda_{pm}}{8J_m} & -\frac{D_m}{J_m} & 0 \end{bmatrix}, \quad (6)$$

$$\mathbf{B}_c = \begin{bmatrix} \frac{1}{L_s} & 0 & 0 \\ 0 & \frac{1}{L_s} & 0 \end{bmatrix}^T, \quad (7)$$

$$\mathbf{C}_c = \begin{bmatrix} 1 & 0 & 0 \\ 0 & 0 & 1 \end{bmatrix}, \quad (8)$$

$$\mathbf{E}_c = \begin{bmatrix} 0 & 0 & \frac{1}{J_m} \end{bmatrix}^T, \quad (9)$$

being D_m the friction coefficient [Nms], J_m the moment of inertia [kgm²], R_s the stator resistance [Ω], L_s the equivalent phase inductance [H], N_p the poles number, and Λ_{pm} the permanent magnetic flux [Wb].

B. Motor operation limits

In the steady-state, the motor behavior follows

$$\tilde{V}_s = \Lambda_{pm}\omega_{e,ss} + (R_s + j\omega_{e,ss}L_s)\tilde{I}_s \quad (10)$$

where \tilde{V}_s is the peak steady-state voltage phasor, $\tilde{I}_s = I_d$ is the peak steady-state current phasor, and $\omega_{e,ss}$ is the steady-state electrical speed. The \tilde{V}_s and $\tilde{I}_s = I_q + jI_d$ phasors are referred to back-electromotive force phasor and $j = \sqrt{-1}$.

Assuming the maximum torque per ampere operation (MTPA), for the surface PMSM, we have that $I_d = 0$, which implies $\tilde{I}_s = I_q = I_{s,max}$. Therefore, all the current is applied in torque generation, and the motor behavior follows that

$$|V_{s,max}|^2 = (\omega_{e,ss}\Lambda_{pm} + R_sI_{s,max})^2 + (\omega_{e,ss}L_sI_{s,max})^2. \quad (11)$$

Condition (11) implies a situation where maximum speed is achieved under full load.

Assuming the limit field weakening condition, we have that $I_q \approx 0$, which implies

$$|V_{s,max}|^2 \approx \left(\frac{\omega_{e,ss}\Lambda_{pm}}{\sqrt{2}} - \omega_{e,ss}L_sI_d \right)^2 + (R_sI_d)^2. \quad (12)$$

Condition (12) presents the relation between I_d and $\omega_{e,ss}$. Therefore, we can obtain the machine absolute maximum speed from the minimum I_d possible. Also, from a given speed, we can calculate the I_d needed to reach that speed. In such case, we get:

$$I_d \approx -\frac{\sqrt{U_x} - L_s\Lambda_{pm}\omega_{e,ss}^2}{R_s^2 + (\omega_{e,ss}L_s)^2} \quad (13)$$

with

$$U_x = [(L_sV_{s,max})^2 - (R_s\Lambda_{pm})^2]\omega_{e,ss}^2 + (R_sV_{s,max})^2. \quad (14)$$

C. Motor model in discrete-time

To further apply MPC, we need to obtain a discrete-time model of the PMSM.

Therefore, it is necessary to linearize the continuous model around an operation point. For the application in MPC, a zero-order linearization is enough. Thus, we define $\omega_{e,op}$ as a constant value defined by the controller design.

Next, a discretization method is required. We prefer exact discretization, also known as zero-order hold (ZOH), as it provides more detailed information for the MPC. Typically, in motor control applications, the controller design uses first-order Euler discretization. However, this approximation omits the effect of the applied voltages on the speed in the subsequent control step. Exact discretization retains this information. The downside is that the model is limited to the operating point for which this discretization is applied. To perform exact discretization, we need to apply:

$$\mathbf{A} = e^{\mathbf{A}_c(\mathbf{x}_{op})T_s} \in \mathbb{R}^{n \times n} \quad (15)$$

$$\mathbf{B} = \mathbf{A}_c^{-1}(\mathbf{x}_{op})(\mathbf{A} - \mathbf{I}_n)\mathbf{B}_c \in \mathbb{R}^{n \times n_u} \quad (16)$$

$$\mathbf{C} = \mathbf{C}_c \in \mathbb{R}^{n_y \times n} \quad (17)$$

where T_s is the sampling time and I_n is an identity matrix of order n (open-loop process order), and n_u is the number of inputs and n_y is the number of outputs.

D. Inverter model

We model the inverter considering ideal switches. Therefore, the three-phase voltages produced by the inverter are described by:

$$\begin{bmatrix} v_{as}(t) \\ v_{bs}(t) \\ v_{cs}(t) \end{bmatrix} = \frac{v_{dc}(t)}{3} \begin{bmatrix} 2 & -1 & -1 \\ -1 & 2 & -1 \\ -1 & -1 & 2 \end{bmatrix} \begin{bmatrix} \gamma_{as}(t) \\ \gamma_{bs}(t) \\ \gamma_{cs}(t) \end{bmatrix} \quad (18)$$

where γ_{as} , γ_{bs} and γ_{cs} are the switches command and v_{dc} is the dc-link voltage.

The dc-link current is given by:

$$i_{dc}(t) = i_{rect}(t) - (i_{as}(t)\gamma_{as}(t) + i_{bs}(t)\gamma_{bs}(t) + i_{cs}(t)\gamma_{cs}(t)) \quad (19)$$

where $i_{rect}(t)$ is the bus supply current. Therefore, the dc-link dynamic is given by:

$$\frac{dv_{dc}(t)}{dt} = \frac{i_{dc}(t)}{C_{dc}} \quad (20)$$

where the C_{dc} is the dc-link capacitance.

If sinusoidal pulse-width modulation (SPWM) is used, overmodulation may be necessary to reach the motor limit conditions.

III. INTEGRAL CCS-MPC TO LINEAR PROCESSES

When designing an MPC, we first obtain an open-loop prediction model of the process. We then propose a cost functional that indicates what aspects the control should penalize. Finally, we determine the control action by minimizing the cost functional subject to the prediction model and any other constraints.

In this paper, we use a State-Space MPC without constraint treatment. This means the open-loop prediction model of the process is based on a state-space open-loop model of the process. This prediction model contains information about N future steps, where N is the prediction horizon. Furthermore, the only constraint considered in the control design is the prediction model itself. The cost functional penalizes the tracking error, the control action, and the accumulated error of outputs. This third term is uncommon in predictive controls, but it enhances the control wide-band tracking capability, giving the control integral action. Therefore, we call this control as Integral Convex Control Set MPC (ICCS-MPC). Consequently, the cost functional is given by

$$\mathcal{J}(\hat{\mathbf{u}}_{seq}) = (\hat{\mathbf{y}}_{seq} - \hat{\mathbf{y}}_{seq})^T \mathbf{W}_y (\hat{\mathbf{y}}_{seq} - \hat{\mathbf{y}}_{seq}) + \hat{\mathbf{u}}_{seq}^T \mathbf{W}_u \hat{\mathbf{u}}_{seq} + \hat{\mathbf{z}}_{seq}^T \mathbf{W}_z \hat{\mathbf{z}}_{seq} \quad (21)$$

whereas the prediction model can be written as:

$$\hat{\mathbf{y}}_{seq}(\hat{\mathbf{u}}_{seq}) = \mathbf{H}\hat{\mathbf{u}}_{seq} + \mathbf{Q}\mathbf{x}(k) \in \mathbb{R}^{Nn_y \times 1} \quad (22)$$

with

$$\hat{\mathbf{y}}_{seq}(k+N|k) = \begin{bmatrix} \hat{\mathbf{y}}(k+1|k) \\ \hat{\mathbf{y}}(k+2|k) \\ \vdots \\ \hat{\mathbf{y}}(k+N|k) \end{bmatrix} \in \mathbb{R}^{Nn_y \times 1} \quad (23)$$

$$\hat{\mathbf{u}}_{seq}(k+N-1|k) = \begin{bmatrix} \mathbf{u}(k) \\ \hat{\mathbf{u}}(k+1|k) \\ \vdots \\ \hat{\mathbf{u}}(k+N-1|k) \end{bmatrix} \in \mathbb{R}^{Nn_u \times 1} \quad (24)$$

$$\mathbf{H} = \begin{bmatrix} \mathbf{CB} & \mathbf{0} & \dots & \mathbf{0} \\ \mathbf{CAB} & \mathbf{CB} & \dots & \mathbf{0} \\ \vdots & \vdots & \ddots & \vdots \\ \mathbf{CA}^{N-1}\mathbf{B} & \mathbf{CA}^{N-2}\mathbf{B} & \dots & \mathbf{CB} \end{bmatrix} \in \mathbb{R}^{Nn_y \times Nn_u} \quad (25)$$

$$\mathbf{Q} = [\mathbf{CA} \quad \mathbf{CA}^2 \quad \dots \quad \mathbf{CA}^N]^T \in \mathbb{R}^{Nn_y \times Nn} \quad (26)$$

with the future reference sequence being

$$\hat{\mathbf{y}}_r = \begin{bmatrix} \hat{\mathbf{y}}_r(k+1|k) \\ \hat{\mathbf{y}}_r(k+2|k) \\ \vdots \\ \hat{\mathbf{y}}_r(k+N|k) \end{bmatrix} \in \mathbb{R}^{Nn_y \times 1} \quad (27)$$

and the predicted accumulative error sequence given by

$$\hat{\mathbf{z}}_{seq} = \begin{bmatrix} \hat{\mathbf{z}}(k+1|k) \\ \hat{\mathbf{z}}(k+2|k) \\ \vdots \\ \hat{\mathbf{z}}(k+N|k) \end{bmatrix} \in \mathbb{R}^{Nn_y \times 1} \quad (28)$$

whereas

$$\hat{\mathbf{z}}(k+1) = \mathbf{z}(k) + \hat{\mathbf{y}}_r(k+1) - \hat{\mathbf{y}}(k+1), \quad (29)$$

and $\mathbf{W}_y \in \mathbb{R}^{Nn_y \times Nn_y}$, $\mathbf{W}_u \in \mathbb{R}^{Nn_u \times Nn_u}$ and $\mathbf{W}_z \in \mathbb{R}^{Nn_y \times Nn_y}$ are the matrices that consider multiple tracking penalties \mathbf{w}_y , \mathbf{w}_u and \mathbf{w}_z for the error of the predicted output signals $\hat{\mathbf{y}}$ in relation to the future reference signals $\hat{\mathbf{y}}_r$, the sequence of predicted control actions $\hat{\mathbf{u}}$ and the predicted accumulated error $\hat{\mathbf{z}}$, respectively. We assume the same penalty exists for the same variable in any future step. Also, we assume that \mathbf{W}_y , \mathbf{W}_u and \mathbf{W}_z are diagonal matrices. However, the penalty can be different for different outputs in $\hat{\mathbf{y}}$, for example.

By minimizing (21) subject to (22) with respect to the variable $\hat{\mathbf{u}}_{seq}$ and selecting the terms of $\hat{\mathbf{u}}_{seq}$ at instant k , we obtain the control action $\mathbf{u}(k)$. We apply only the terms at instant k from the sequence and recalculate the entire sequence at the next sampling time. This procedure, known as receding horizon, defines the control as MPC. In the case we are analyzing, the control action is given by [14]

$$\mathbf{u}(k) = \mathbf{K}_x \mathbf{x}(k) - \mathbf{K}_z \mathbf{z}(k) + \mathbf{K}_r \hat{\mathbf{y}}_{seq} \in \mathbb{R}^{n_u \times 1} \quad (30)$$

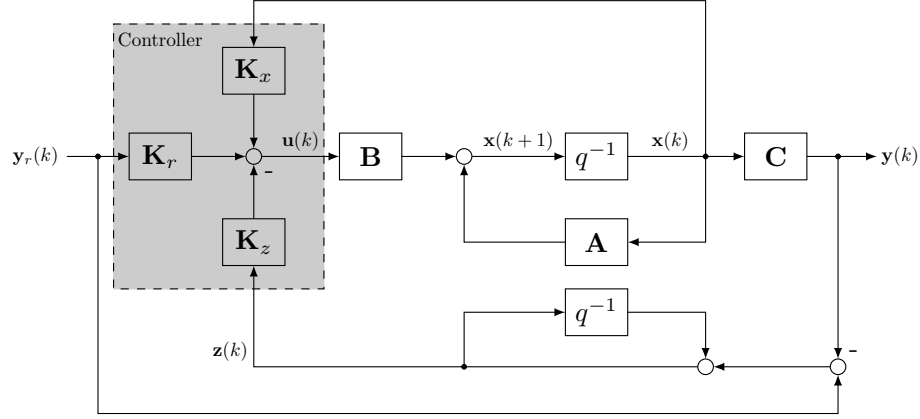


FIGURE 1. ICCS-MPC block-diagram. The omitted operators in the connectors are additions.

with

$$\mathbf{K}_x = \mathbf{K}[\mathbf{Q}^T \mathbf{W}_y \mathbf{H} + (\mathbf{T}_N \mathbf{Q})^T \mathbf{W}_z \mathbf{T}_N \mathbf{Q}]^T \in \mathbb{R}^{n_u \times n}$$

$$\mathbf{K}_z = \mathbf{K}(\mathbf{W}_z \mathbf{T}_N \mathbf{H})^T \in \mathbb{R}^{n_u \times n_y}$$

$$\mathbf{K}_r = \mathbf{K}(\mathbf{W}_y \mathbf{H} + \mathbf{T}_N^T \mathbf{W}_z \mathbf{T}_N \mathbf{H})^T \in \mathbb{R}^{n_u \times n_y N}$$

$$\mathbf{K} = \mathbf{I}_0 [\mathbf{H}^T \mathbf{W}_y \mathbf{H} + \mathbf{W}_u + (\mathbf{T}_N \mathbf{H})^T \mathbf{W}_z \mathbf{T}_N \mathbf{H}]^{-1} \in \mathbb{R}^{n_u \times n_u N}$$

$$\mathbf{I}_0 = \begin{bmatrix} \mathbf{I}_N & \mathbf{0} & \dots & \mathbf{0} \end{bmatrix} \in \mathbb{R}^{n_u \times n_u N}$$

$$\mathbf{T}_N = \begin{bmatrix} \mathbf{I}_y & \mathbf{0} & \dots & \mathbf{0} \\ \mathbf{I}_y & \mathbf{I}_y & \dots & \mathbf{0} \\ \vdots & \vdots & \ddots & \vdots \\ \mathbf{I}_y & \mathbf{I}_y & \mathbf{I}_y & \mathbf{I}_y \end{bmatrix} \in \mathbb{R}^{N n_y \times N n_y}$$

$$\mathbf{I}_y = \begin{bmatrix} 1 & 0 & \dots & 0 \\ 0 & 1 & \dots & 0 \\ \vdots & \vdots & \ddots & \vdots \\ 0 & 0 & 0 & 1 \end{bmatrix} \in \mathbb{R}^{n_y \times n_y}$$

and $\mathbf{0}$ are matrices of zeros from the respective order.

The control law from (30) has three clear different components: the first penalizes the process states, being a feedback state action; the second penalizes the accumulative error, being an integral action; and, the third penalizes (or filters) the reference, being a feedforward-like action. Figure 1 presents a block-diagram for control action calculation.

IV. DESIGN RULES FOR ICCS-MPC TO SPMSM

The MPC strategy proposed in Section III has several terms to choose for designing the cost functional. Therefore, choosing those terms implies what is optimal in the control design. A wrong choice can yield the closed-loop system to a “bad” performance from a human being perspective or even to instability. Thus, in this section, we present a design guide to apply the control strategy from Section III in a surface PMSM.

We can now particularize the control design considering the model shown in Section II. Therefore, we have:

$$\mathbf{x}(k) = [i_{ds}(k) \quad i_{qs}(k) \quad \omega_e(k)]^T, \quad (31)$$

$$\mathbf{y}(k) = [i_{ds}(k) \quad \omega_e(k)]^T, \quad (32)$$

$$\mathbf{u}(k) = [v_{ds}(k) \quad v_{qs}(k)]^T, \quad (33)$$

$$\mathbf{y}_r(k) = [i_{ds,r}(k) \quad \omega_{e,r}(k)]^T, \quad (34)$$

$$\mathbf{z}(k) = [i_{ds,z}(k) \quad \omega_{e,z}(k)]^T. \quad (35)$$

Besides the prediction horizon N , the tuning parameters are:

$$\mathbf{w}_y = \text{diag}([\rho_{i_{ds}} \quad \rho_{\omega_e}]) \quad (36)$$

$$\mathbf{w}_u = \text{diag}([\rho_{v_{ds}} \quad \rho_{v_{qs}}]) \quad (37)$$

$$\mathbf{w}_z = \text{diag}([\rho_{i_{ds,z}} \quad \rho_{\omega_{e,z}}]). \quad (38)$$

The following subsections present rules for designing the control.

A. Linearized model

The first step is to obtain the linearization model, in a speed operation point. We suggest linearizing about the middle of the maximum motor speed.

B. Normalization

We define the weighting factor of control action as:

$$\mathbf{w}_u = (\mathbf{CB})^T \bar{\mathbf{w}}_u (\mathbf{CB}) \quad (39)$$

being $\bar{\mathbf{w}}_u$ the normalized weighting factor of control action, given by

$$\bar{\mathbf{w}}_u = \text{diag}([\bar{\rho}_{v_{ds}} \quad \bar{\rho}_{v_{qs}}]). \quad (40)$$

For $\mathbf{w}_z = \mathbf{0}$, $\mathbf{w}_y = \mathbf{I}_y$, and $\bar{\mathbf{w}}_u = \mathbf{I}_y$ we normalize the cost function, being the same penalization for the control action and the tracking error [19]. Hence, we can use the other weighting factors on the same scale. It is important to note that \mathbf{w}_u matrix is not necessarily diagonal due to the normalization.

C. Adjusting tracking penalization

For the control application in the PMSM, the control designer just needs to guarantee $\rho_{\omega_e} \geq \rho_{i_{ds}}$ to ensure priority in the speed tracking. The control will work if ρ_{ω_e} is a slightly smaller than $\rho_{i_{ds}}$, but choosing ρ_{ω_e} much smaller than $\rho_{i_{ds}}$ will cause instability in the closed-loop control. For simplicity, we can just maintain $\mathbf{w}_y = \mathbf{I}_y$.

D. Adjusting accumulative error penalization

In this case, it is better to ensure the integral penalization in the smaller value that attends the steady-state tracking. It is better, as well, if $i_{ds,z}$ penalization is higher than the $\omega_{e,z}$ penalization. The control designer can start with both $\rho_{i_{ds,z}}$ and $\rho_{\omega_{e,z}}$ in low values and rising then or he could start $\mathbf{w}_z = \mathbf{I}_y$ and reduce $\rho_{\omega_{e,z}}$ for example.

E. Adjusting control action penalization

The most important adjustment after normalization is the control action penalization. These parameters regulate the controller bandwidth, controlling the energy expended on the plant. Consequently, high values for $\bar{\rho}_{v_{ds}}$ and $\bar{\rho}_{v_{qs}}$ will slow the dynamic response of the closed-loop system. Conversely, low values for $\bar{\rho}_{v_{ds}}$ and $\bar{\rho}_{v_{qs}}$ will accelerate the closed-loop dynamics. However, with normalization, choosing $\bar{\mathbf{w}}_u = \mathbf{I}_y$ will result in a considerably fast response. Even $\bar{\mathbf{w}}_u = 100\mathbf{I}_y$ will yield a fast closed-loop response if the other parameters are close to unity.

Penalization can be the same for v_{ds} and v_{qs} , but usually, the penalization for v_{ds} can be considerably lower to ensure a fast i_{ds} response. The control designer can set $\bar{\rho}_{v_{ds}} = 10$, for example.

One way to choose $\bar{\rho}_{v_{qs}}$ is by analyzing the expected closed-loop frequency response of the speed to its reference. The control designer can adjust $\bar{\rho}_{v_{qs}}$ by an order of magnitude and analyze the changes in bandwidth.

Some responses seen in simulation are faster than what is achievable in practice. Analyzing the obtained gains is also important since high gains can cause variable overflow in a microcontroller. This will be clarified in Section V.

V. CONTROL DESIGN EXAMPLE

This section presents an example for designing the control for a PMSM.

The PMSM parameters and rated values are presented in Table 1. We suppose inverter operation in the non-overmodulated region to focus on the control performance with linear control action. Therefore, the maximum values for the motor can not be achieved.

The first step is to obtain the discrete linearized model. We linearize around 240 rad/s (electrical) since this operating point is in the middle of the speed range in the MTPA region (the lower limit is 0 and the upper limit is approximately 480 rad/s, equivalent to 20 rad/s mechanical or 200 rpm).

Next, we normalize the control penalization, define $N = 2$, and evaluate the motor closed-loop response for

TABLE 1. Motor Parameters and Rated Values

Parameter	Value	Rated Value	Value (O.M./N.O.M)
R_s	15.5 Ω	Speed	200/190 rpm
L_s	0.038 H	Torque	27/20 Nm
J_m	0.0522 kg m ²	Voltage (RMS)	127/110 V
D_m	9.8·10 ⁻⁴ N m s	Current (RMS)	2.3/1.62 A
Λ_{pm}	0.233 Wb	Power	475/360 W
T_s	100 μ s	Sw. Freq.	10 kHz
N_p	48 poles	DC-link	311 V

O.M. : Overmodulated, N.O.M. : Non-Overmodulated

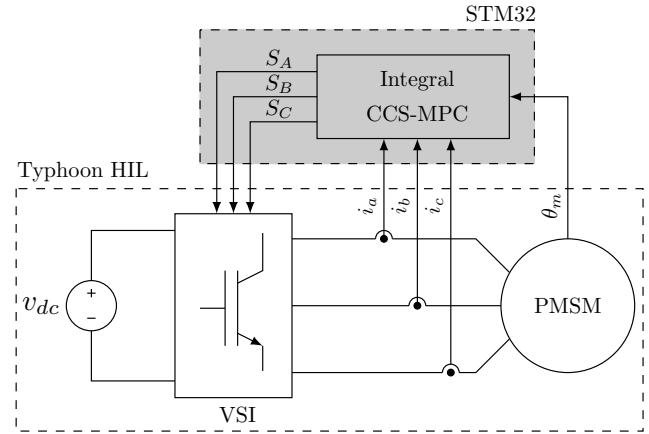


FIGURE 2. Schematic of the implementation

$i_{ds,r} = 0$ A, considering $\mathbf{w}_y = \mathbf{I}_y$, $\bar{\mathbf{w}}_u = 100\mathbf{I}_y$ (this condition is chosen because tuning at unity makes the control action significantly affected by commutation noise), and $\mathbf{w}_z \approx \mathbf{0}$. We gradually increase $\rho_{i_{ds,z}}$ and $\rho_{\omega_{e,z}}$ until steady-state tracking is achieved for $i_{ds,r}$ and $\omega_{e,r}$, with $\rho_{i_{ds,z}} = 1$ and $\rho_{\omega_{e,z}} = 0.01$.

Finally, we define three controllers for testing: Controller 0 ($\rho_{v_{qs}} = 10^3$), Controller 1 ($\rho_{v_{qs}} = 10^4$), and Controller 2 ($\rho_{v_{qs}} = 10^5$), and evaluate the motor response for these three tunings. In all cases, we maintain $\rho_{v_{ds}} = 10^2$ since the i_{ds} correction involves lower voltage values than the speed correction, and the control should have more freedom to correct the i_{ds} error. Controllers with $\rho_{v_{qs}} < 10^3$ are significantly affected by commutation noise.

VI. METHODS

The experimental results are obtained using Hardware-in-the-Loop (HiL) simulation on a real-time simulator platform from Typhoon HIL, model HIL404. The motor and the inverter are embedded in the Typhoon HIL platform and are emulated in real time with a resolution of 1.0 μ s. Figure 2 shows the schematic used in the HiL implementation.

The designed controllers (Controller 0, Controller 1 and Controller 2 presented in Section V) are implemented in the microcontroller STM32F767ZI using development board NUCLEO-F767ZI. The microcontroller has an ARM-m7

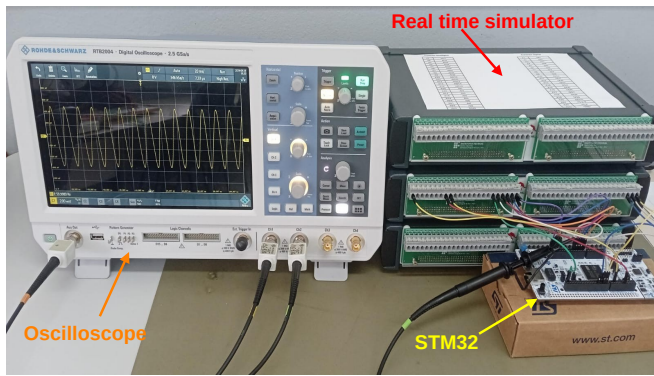


FIGURE 3. Experimental setup

core, native floating point unit and 216 MHz CPU. Figure 3 shows the experimental setup.

The results were selected to evaluate the controllers performance in different scenarios: conventional speed tracking, with ramp references and disturbance rejection; incremental step references, with power tracking analysis; sinusoidal references, to ac tracking analysis; experimental Bode diagram, to observe the control bandpass width. This last result was obtained using a Rohde&Schwarz RTB2004 oscilloscope.

All the data was collect using Typhoon HIL SCADA software, at 100 μ s sampling rate.

VII. RESULTS AND DISCUSSION

This section presents the results and discussion regarding the controllers designed in the previous sections. Additionally, it explores the application of ICCS-MPC in comparison to FCS-MPC, highlighting their relative performance. Furthermore, it provides an analysis of the computational cost associated with each approach.

A. Results and discussion involving designed controllers for speed tracking

Figure 4 presents the speed dynamic response for the three designed controllers. A load torque of 20 Nm is applied to the motor at 0.5 s and removed at 1.25 s. In all cases, the closed-loop speed can track the reference, except in maximum speed and load, due to the voltage limit. Controllers 0 and 1 have faster disturbance rejection than Controller 2 which is visibly slower, as expected from the control design. As expected, Controller 0 is more sensitive to the inverter noise than the others since it has the lowest $\bar{\rho}_{v_{qs}}$. The high variance in Controller 0 voltage is significantly influential, causing it to remain nearly saturated most of the time, oscillating between saturation states. This substantial variance also leads to noisier currents compared to those observed in other responses. Despite these fluctuations, $i_{ds,r}$ tracking is successfully achieved as anticipated under the given design conditions. As there is no feedback linearization decoupling in this controller, some impact is seen on the i_{ds} dynamics during the transitions. We stand out that the control naturally penalizes the cross-coupling dynamic with the

feedback action (\mathbf{K}_x gain). Controller 1 is also susceptible to noise but with significantly lower intensity than Controller 0. Controller 2 has high noise rejection but it has a slower speed dynamic response and slower disturbance rejection.

In Fig. 5, we see an increasing step test to all controllers. The full load (20 Nm) is inserted at 1.5 s. The i_{qs} behavior (which is proportional to the electromagnetic torque) clearly shows this load insertion and all the controllers' responses to provide enough current. Due to the high noise sensitivity, Controller 0 has encounters difficulty of high-speed reference tracking as it frequently enters saturation regions. Controllers 1 and 2 can reject disturbances even in the high-speed references. However, Controller 1 saturates more frequently than Controller 2, which only approximates itself from voltage saturation near the actual voltage limit of the non-overmodulated motor-inverter system. In all cases, we see the reduction in v_{ds} value to maintain i_{ds} in the null reference, which guarantees the MTPA condition. Therefore, in the maximum speed and load condition, the machine operates in the rating condition. Controller 2 is the best to provide steady-state operation at full power. However, this same controller had the worst disturbance rejection, and the slower transient response at each speed step. Besides this transient response can be considered satisfactory.

Figure 6 presents the speed tracking for a sinusoidal reference of 10 Hz. This test is performed to evaluate the transient response of the controllers. Controller 0 and Controller 1 were capable to allow the motor tracking of the 10 Hz sinusoidal reference. Therefore, these controllers have at least 10 Hz bandwidth. However, like in the other tests, Controller 0 has high noise sensitivity, and it has even v_{ds} peaks besides v_{qs} constant saturation. Controller 1 has similar performance with less noise sensitivity. It indicates that Controller 1 has more attenuation than Controller 0 at high frequencies, which indicates latter's larger bandwidth. Controller 2 was not capable to allow speed tracking at 10 Hz reference. Therefore, this controller has a reduced bandwidth when compared with Controller 0 and Controller 1. This condition justifies Controller 2 high noise rejection since we can suppose high attenuation at high frequencies.

B. Bandwidth Analysis

Figure 7 presents the experimental Bode Diagram for Controllers 0 and 1. We are unable to perform Controller 2 frequency analysis due to its low bandwidth. These Bode Diagrams are formulated considering the speed as output and the speed reference as input, for $i_{ds,r} = 0$. In Fig. 7, Controller 0 allows about 100 Hz tracking bandwidth, with a small resonance about 70 Hz. The phase tends to 270° in high frequencies. Controller 1 allows about 40 Hz bandwidth. The closed-loop starts with phase delays from values lower than 10 Hz. It is seen some anomalies close to 1 kHz due sampling problems at these frequencies.

These experimental closed-loop Bode Diagrams show the speed tracking capabilities of the closed-loop systems, in

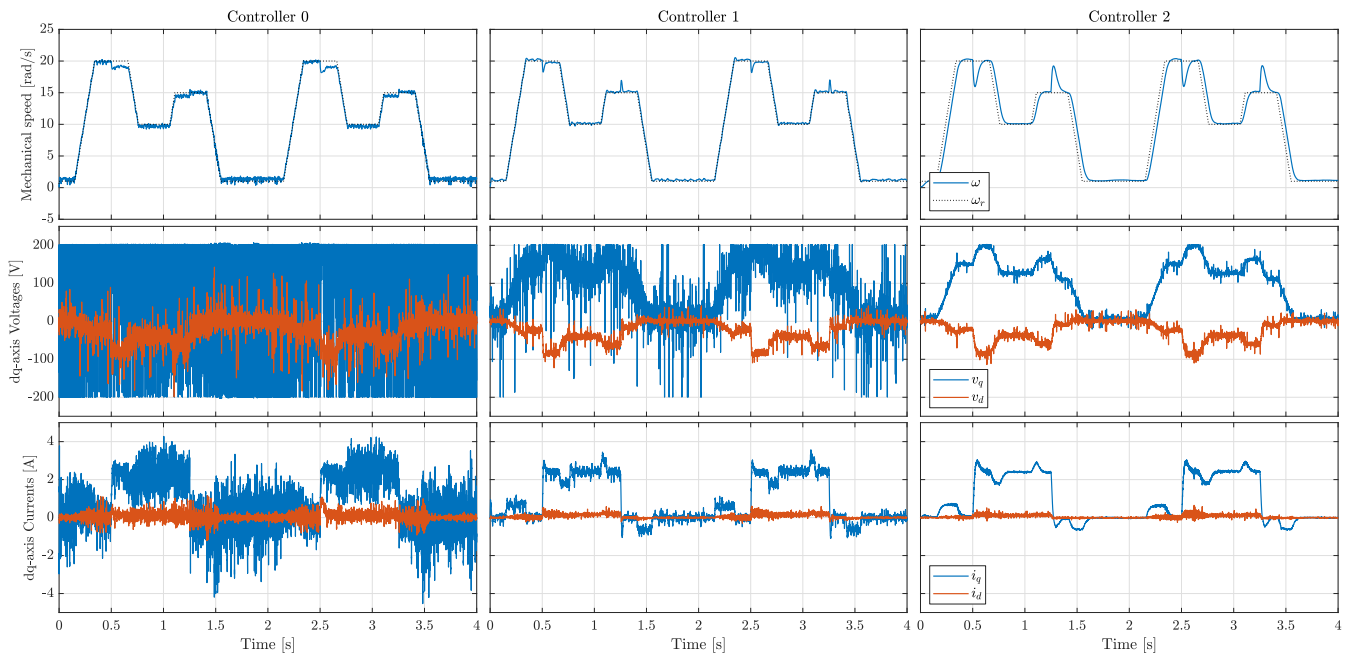


FIGURE 4. Speed Tracking Test with load disturbance rejection for different controllers, presenting mechanical speed, dq -voltages and dq -currents for each case

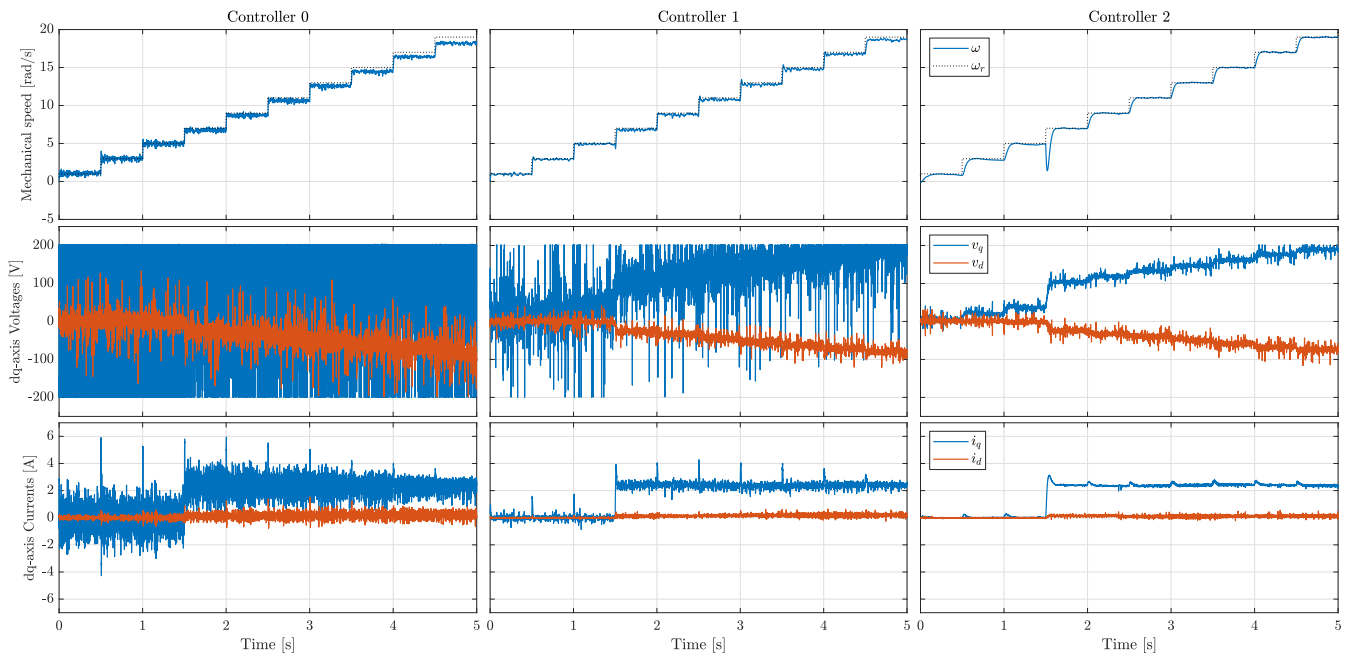


FIGURE 5. Speed Tracking with sequence of step references and full-load for different controllers, presenting mechanical speed, dq -voltages and dq -currents for each case

relation to the speed reference. However, they do not show directly the noise influence over the control action. They show clearly that Controller 0 has a larger bandwidth than the others, still it should have high attenuation at high frequencies, considering that these are high frequencies of speed references. In fact, Controller 2 has a smaller bandwidth and it has low noise sensitivity from other signals. Controller 0 and Controller 1 have a larger bandwidth than Controller 2

but they are significantly more affected by the inverter noise. This sensitivity is not expected from the Bode Diagram analysis in a first view, but this frequency analysis is not a sufficient index to explain this noise sensitivity. What the bode-diagram says is that there is a direct relation between the $\tilde{\rho}_{v_{qs}}$ tuning (open-loop weighting) and the closed-loop speed bandwidth, which is an important relation for the control design. With this single parameter, it is possible

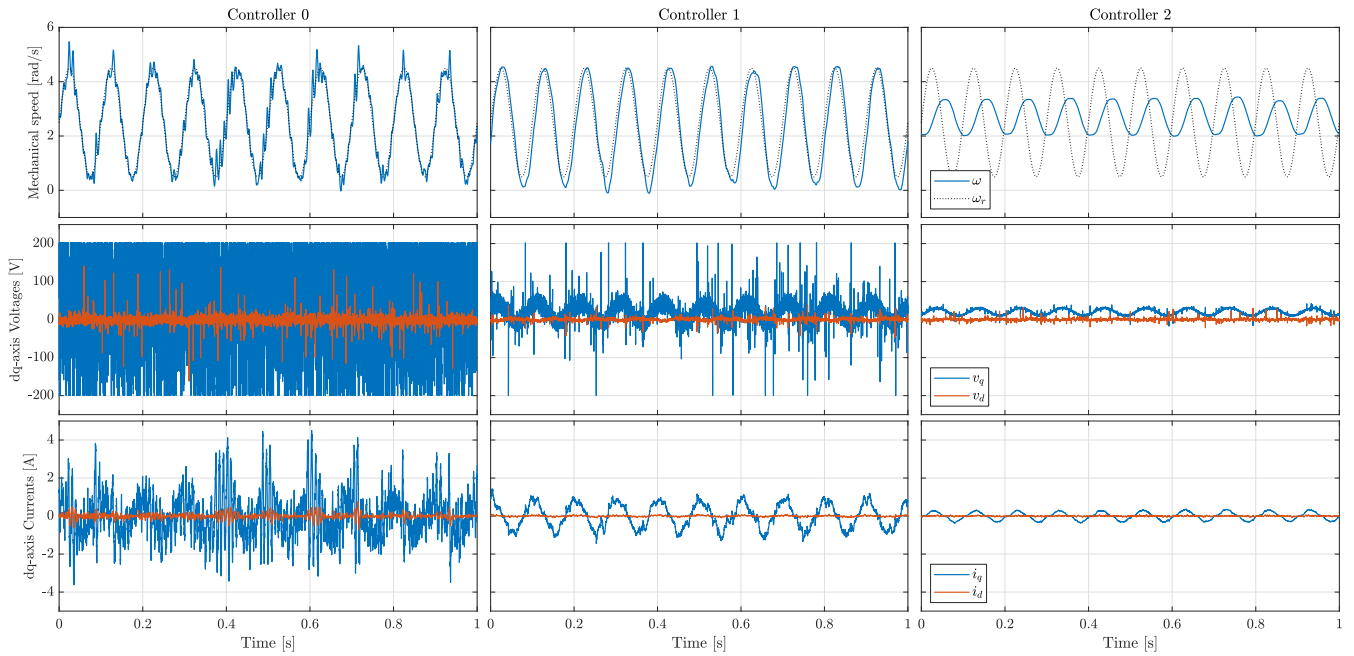


FIGURE 6. Sinusoidal Speed Tracking Test for evaluating different controllers bandwidth, presenting mechanical speed, dq -voltages and dq -currents for each case

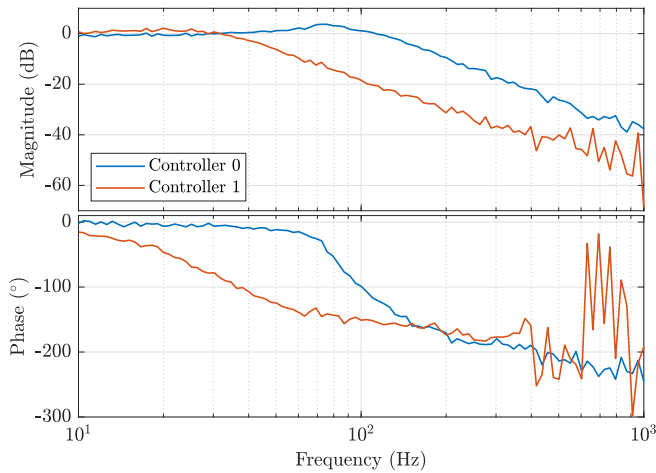


FIGURE 7. Experimental Closed-loop Bode Diagram for Controllers 0 and 1 (both with more than 10 Hz cut-off frequency)

to evaluate the closed-loop bandwidth frequency. However, as the bandwidth increases, so does the noise sensitivity, which is not directly reflected in the closed-loop frequency response.

C. Torque Analysis

Figure 8 presents the torque-speed relation for the test observed in Fig. 5, from 7 rad/s (when the load torque is inserted). It shows that the steady-state torque has a considerably larger ripple when Controller 0 is applied due to the noise sensitivity of this controller. Even the transitions, which are faster, require high torque quantities, close to the power limits. The motor can provide these requirements

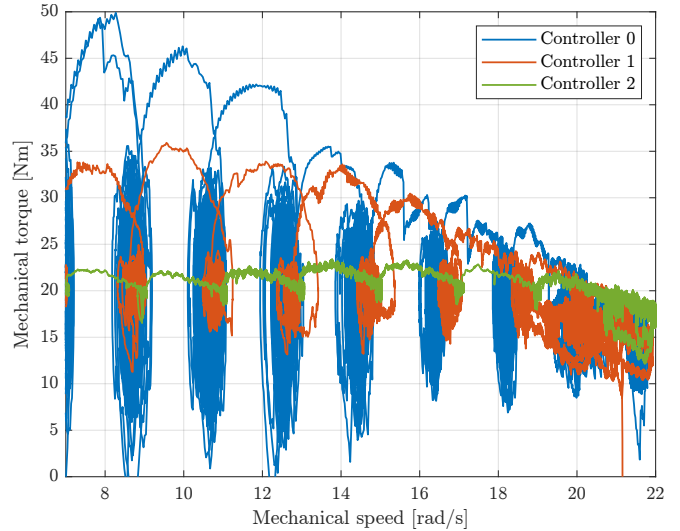


FIGURE 8. Torque per speed characteristic for different controllers

in lower speeds since they are more distant to the motor power limit. In high speeds, the transitions are slower, because the motor can not provide the required torque due to the power limit. It characterizes the PMSM nonlinear behavior. Controller 1 has a lower torque requirement for transitions than Controller 0. However, it has also high torque demands (closed to the rated torque) and, at high speeds, the torque transitions are reduced. Controller 2 has smoother transitions that require a small extra-torque. Also, the steady-state torque has small ripple for Controller 2. The relation of torque-speed for this controller is practically flat. All the controllers have a torque reduction when the maximum speed

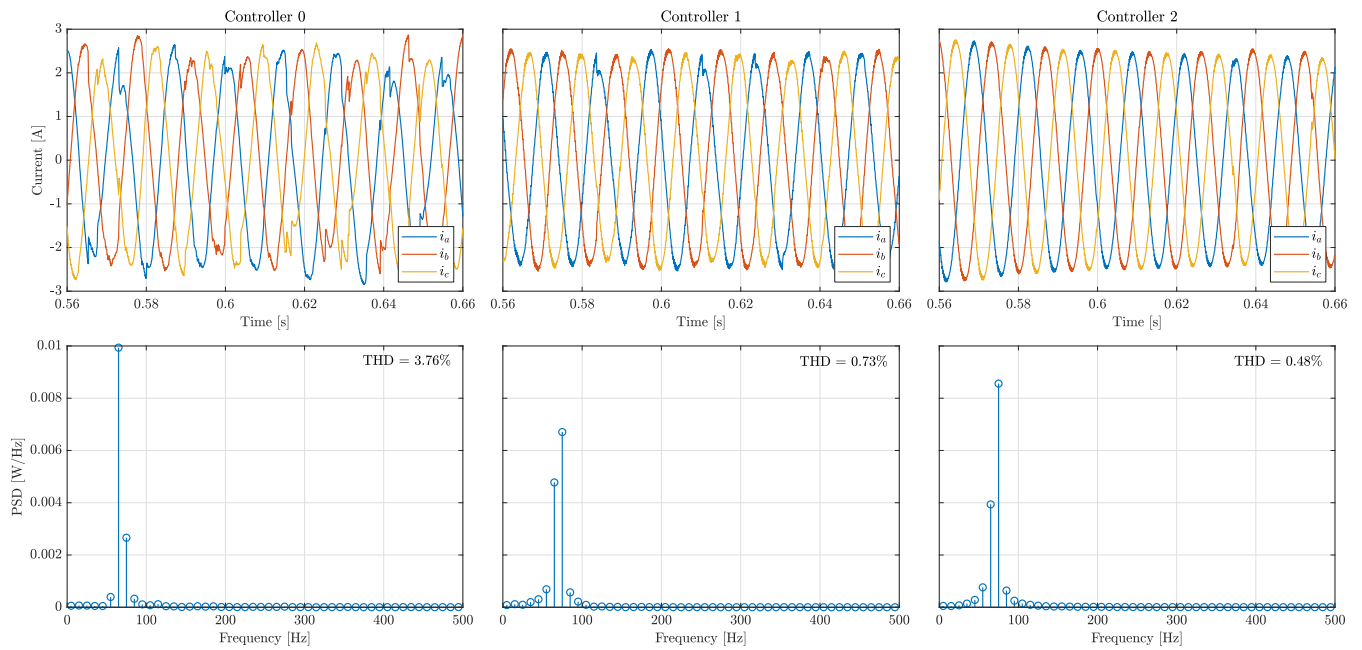


FIGURE 9. Current in function of the time and Power spectrum density (PSD) for the same current in steady-state for maximum speed with the load torque applied, in the same speed tracking test presented in Fig. 4 for each controller

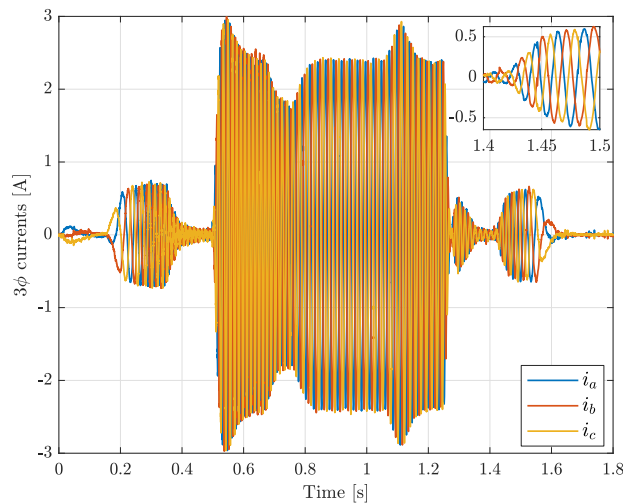


FIGURE 10. Three-phase currents for speed tracking test from Fig. 4 for Controller 2

is reached and the power limit is saturated. However, Controller 2 has a higher average torque since it has lower noise. This condition explains why it rejects better the disturbance in the high speeds in the test observed in Fig. 5. Another factor seen in Fig. 5 is the presence of the i_{qs} spikes. These spikes are directly correlated with the torque transients seen in the Fig. 8. Considering the exposed, a controller tuned with $\bar{\rho}_{v_{qs}}$ between the values used for Controller 1 and Controller 2 could be ideal for this specific application, likely providing a bandwidth of about 10 Hz. Among the proposed controllers, Controller 2 can be considered the best due to its lower noise sensitivity and better torque-per-speed

ratio, despite having a lower bandwidth than the others. If a larger bandwidth is required, Controller 1 is preferable over Controller 0, as Controller 0 operates near saturation almost all the time due to its aggressive characteristics.

D. Current analysis

Figure 9 presents current in function of the time and Power Spectrum Density (PSD) for the same current in steady-state for maximum speed with the load torque applied, in the same speed tracking test presented in Fig. 4 for each controller.

We observe that all controllers provide quasi-sinusoidal currents in the time domain by Fig. 9. Considering all PSD results, presented in Fig. 9, we see the main power centered on the fundamental frequency. The spectral analysis reveals an absence of significant power density at other frequencies in the spectrum, indicating that the current exhibits high quality with minimal harmonic distortion. The low harmonic distortion is also seen the THD (Total Harmonic Distortion) result presented in each PSD result. The presented current distortion has more influence from the VSI usage than the controller by itself since even in the more aggressive configuration the THD is small.

Figure 10 presents the complete three-phase currents for the test presented in Fig. 4 for Controller 0. In Fig. 10, we see that the three-phase currents are separated by 120 electrical degrees. In the detail, we see these currents respected the sinusoidal form when there is load torque and/or a speed transition as expected. It is also noticed current frequency variates with the motor speed, since it is a PMSM.

E. Computational cost results and discussion

Based on tested measurements, the complete interrupt routine requires 60 μs out of the total 100 μs sampling period. Most of this time is consumed by the dq -transformation and ADC operations. Specifically, the ICCS-MPC computation accounts for only 7.76 μs , which represents a significantly smaller fraction of the total sampling period.

F. Discussion on Using ICCS-MPC over FCS-MPC

In power electronics, two primary MPC actuation strategies are widely used. The first involves modulation, characteristic of CCS-MPC. The second directly switches states without modulation, known as FCS-MPC.

The key differences between modulated and unmodulated control strategies define the distinctions between FCS-MPC and the proposed ICCS-MPC. For additional details, see [16], [20], and [7]. In particular, [16] provides a direct comparison of FCS-MPC, FCS-MPC using the ICCS-MPC cost function, and ICCS-MPC itself for $N = 1$, applied to a RL-load. The following discussion summarizes these differences.

1) Advantages and Challenges of Modulated Control

Modulated control, such as CCS-MPC, offers several benefits, such as:

- It maintains a fixed switching frequency, a critical parameter in converter and control system design.
- The fixed frequency simplifies inverter design, enabling accurate estimation of current attenuation relative to the motor bandwidth, and facilitates dc-link and filter design.
- Sampling time and control bandwidth can be aligned, typically limiting the control bandwidth to one-quarter of the switching frequency to comply with the Nyquist-Shannon sampling theorem.
- In microcontroller (MCU) implementations, the use of PWM peripherals ensures synchronization between interrupt timings and ADC operations.
- The fixed switching frequency ensures consistent noise characteristics that can be mitigated with higher switching frequencies.
- Modulated control typically produces smoother current profiles and reduces torque ripple compared to unmodulated strategies.

Despite these advantages, the use of a fixed frequency introduces constant-frequency noise, which, while predictable, requires careful design to manage effectively.

2) Advantages and Challenges of Unmodulated Control

Unmodulated control, such as FCS-MPC, has distinct characteristics:

- It does not operate at a fixed switching frequency, resulting in a variable range of action.
- In digital control systems, the maximum effective switching frequency is limited to half the interrupt rate [4].
- For small motors with low inductance, this variability can result in greater current distortion and torque ripple compared to modulated approaches at the same interrupt rate [16], [20].
- Lower switching frequencies reduce commutation losses, which is a significant advantage in some applications.
- Filter design becomes more complex as it cannot target a single frequency. Consequently, high-order filters may be required for effective attenuation [21].
- Implementing FCS-MPC in an MCU requires direct digital outputs for switch driving, which can complicate ADC synchronization and current measurement, particularly for small PMSM applications.

3) Philosophical and Computational Considerations

From a design and computational perspective, the differences between ICCS-MPC and FCS-MPC are significant. For example:

- FCS-MPC provides greater flexibility in cost function design and directly incorporates motor nonlinearities. However, this flexibility is constrained by the exponential increase in computational complexity as the prediction horizon increases.
- ICCS-MPC leverages a fixed switching frequency, enabling higher control bandwidth for the same interrupt period and improving current quality and torque ripple performance.
- The computational cost of ICCS-MPC is comparable to that of a PI controller, as it primarily involves matrix operations. In contrast, FCS-MPC requires evaluating multiple future states, leading to significant computational overhead as the prediction horizon increases.
- ICCS-MPC inherently compensates for constant disturbances in direct speed control applications, a capability not present in FCS-MPC without external compensators.

4) Summary of Advantages of ICCS-MPC Over FCS-MPC

The proposed ICCS-MPC offers the following advantages:

- A fixed switching frequency, ensuring predictable and stable system behavior.
- Improved current quality and reduced torque ripple.
- Removal of steady-state errors in direct speed control.
- Simplified implementation on MCUs due to synchronization between ADC and PWM peripherals.
- Lower computational cost for equivalent prediction horizons.

VIII. CONCLUSION

This work presented the application of an integral convex control set MPC (ICCS-MPC) applied to a surface PMSM. We presented a design guide for ICCS-MPC application since it has a considerably high quantity of weighting factors. We reduced the tuning parameters to one main normalized parameter $\bar{\rho}_{v_{qs}}$. The results show the relation between this parameter and the closed-loop bandwidth of the machine speed. Three controllers were tested and dynamic tests were presented with all the controllers. We see the high influence of the noise sensitivity in these controllers and conclude that the controller with the smaller variance in control action can be considered better for this motor application.

ACKNOWLEDGMENTS

This work was supported by Fundação de Amparo à Pesquisa e Inovação do Estado de Santa Catarina (FAPESC) – Termo de Outorga 2023TR001509.

The authors also thank the financial support from CAPES/PROAP/AUXPE DS 1928/2023, Process no. 88881.898694/2023-01 - Programa de Pós-Graduação em Engenharia Elétrica PPGEEL/UEDESC, and from CNPq by Process 310447/2021-6.

AUTHOR'S CONTRIBUTIONS

A. G. BARTSCH: Conceptualization, Data Curation, Formal Analysis, Investigation, Methodology, Project Administration, Software, Supervision, Validation, Writing – Original Draft, Writing – Review & Editing. **R. TRENTINI:** Conceptualization, Data Curation, Funding Acquisition, Project Administration, Resources, Validation, Visualization, Writing – Original Draft, Writing – Review & Editing. **A. NIED:** Funding Acquisition, Resources, Supervision, Writing – Review & Editing. **J. OLIVEIRA:** Supervision, Writing – Review & Editing. **F. FERNANDES:** Conceptualization, Investigation, Validation, Visualization, Writing – Original Draft. **S. F. DELL AGNOLO:** Conceptualization, Investigation, Methodology, Visualization, Writing – Original Draft. **M. S. M. CAVALCA:** Supervision, Writing – Review & Editing.

PLAGIARISM POLICY

This article was submitted to the similarity system provided by Crossref and powered by iThenticate – Similarity Check.

REFERENCES

- [1] J. Rodriguez, M. P. Kazmierkowski, J. R. Espinoza, P. Zanchetta, H. Abu-Rub, H. A. Young, C. A. Rojas, "State of the Art of Finite Control Set Model Predictive Control in Power Electronics", *IEEE Transactions on Industrial Informatics*, vol. 9, no. 2, pp. 1003–1016, May 2013, doi:10.1109/TII.2012.2221469, URL: <http://ieeexplore.ieee.org/document/6317184/>.
- [2] T. Geyer, G. Papafotiou, M. Morari, "Model Predictive Direct Torque Control—Part I: Concept, Algorithm, and Analysis", *IEEE Transactions on Industrial Electronics*, vol. 56, no. 6, pp. 1894–1905, Jun. 2009, doi:10.1109/TIE.2008.2007030, URL: <http://ieeexplore.ieee.org/document/4663721/>.
- [3] R. P. Aguilera, P. Lezana, D. E. Quevedo, "Finite-Control-Set Model Predictive Control With Improved Steady-State Performance", *IEEE Transactions on Industrial Informatics*, vol. 9, no. 2, pp. 658–667, May 2013, doi:10.1109/TII.2012.2211027, URL: <http://ieeexplore.ieee.org/document/6256724/>.
- [4] M. Preindl, S. Bolognani, "Model Predictive Direct Torque Control With Finite Control Set for PMSM Drive Systems, Part 1: Maximum Torque Per Ampere Operation", *IEEE Transactions on Industrial Informatics*, vol. 9, no. 4, pp. 1912–1921, Nov. 2013, doi:10.1109/TII.2012.2227265, URL: <http://ieeexplore.ieee.org/document/6418026/>.
- [5] A. G. Bartsch, G. Hermann Negri, C. R. Scalabrin, M. S. M. Cavalca, A. Nied, J. de Oliveira, "Predictive Control Approach For Permanent Magnet Synchronous Motor Drive", *Eletrônica de Potência*, vol. 20, no. 4, pp. 395–403, Nov. 2015, doi:10.18618/REP.2015.4.2567, URL: <https://journal.sobraep.org.br/index.php/rep/article/view/511>.
- [6] J. Rodriguez, J. Pontt, C. A. Silva, P. Correa, P. Lezana, P. Cortes, U. Ammann, "Predictive Current Control of a Voltage Source Inverter", *IEEE Transactions on Industrial Electronics*, vol. 54, no. 1, pp. 495–503, Feb. 2007, doi:10.1109/TIE.2006.888802, URL: <http://ieeexplore.ieee.org/document/4084698/>.
- [7] C. Bordons, C. Montero, "Basic Principles of MPC for Power Converters: Bridging the Gap Between Theory and Practice", *IEEE Industrial Electronics Magazine*, vol. 9, no. 3, pp. 31–43, Sep. 2015, doi:10.1109/MIE.2014.2356600, URL: <http://ieeexplore.ieee.org/document/7271174/>.
- [8] J. A. Rossiter, *Model-based predictive control*, CRC, Boca Raton, 2003.
- [9] C. E. García, D. M. Prett, M. Morari, "Model predictive control: Theory and practice—A survey", *Automatica*, vol. 25, no. 3, pp. 335–348, May 1989, doi:10.1016/0005-1098(89)90002-2, URL: <https://linkinghub.elsevier.com/retrieve/pii/0005109889900022>.
- [10] E. de Santana, E. Bim, W. do Amaral, "A Predictive Algorithm for Controlling Speed and Rotor Flux of Induction Motor", *IEEE Transactions on Industrial Electronics*, vol. 55, no. 12, pp. 4398–4407, Dec. 2008, doi:10.1109/TIE.2008.2007376, URL: <http://ieeexplore.ieee.org/document/4663815/>.
- [11] M. Preindl, S. Bolognani, "Model Predictive Direct Speed Control with Finite Control Set of PMSM Drive Systems", *IEEE Transactions on Power Electronics*, vol. 28, no. 2, pp. 1007–1015, Feb. 2013, doi:10.1109/TPEL.2012.2204277, URL: <http://ieeexplore.ieee.org/document/6216441/>.
- [12] G. H. Negri, M. S. M. Cavalca, J. de Oliveira, C. J. F. Araújo, L. A. Celiberto, "Evaluation of Nonlinear Model-Based Predictive Control Approaches Using Derivative-Free Optimization and FCC Neural Networks", *Journal of Control, Automation and Electrical Systems*, vol. 28, no. 5, pp. 623–634, Oct. 2017, doi:10.1007/s40313-017-0327-x, URL: <http://link.springer.com/10.1007/s40313-017-0327-x>.
- [13] S. Qin, T. A. Badgwell, "A survey of industrial model predictive control technology", *Control Engineering Practice*, vol. 11, no. 7, pp. 733–764, Jul. 2003, doi:10.1016/S0967-0661(02)00186-7, URL: <https://linkinghub.elsevier.com/retrieve/pii/S0967066102001867>.
- [14] A. de Souza Candido, *Desenvolvimento de estratégias de controle preditivo para aplicações aeronáuticas empregando otimização multi-objetivo*, Ph.D. thesis, Instituto Tecnológico da Aeronáutica, São José dos Campos, SP - Brasil, 2010, URL: http://www.bdita.bibl.ita.br/tesesdigitais/lista_resumo.php?num_tese=000557937.
- [15] A. G. Bartsch, G. H. Negri, M. S. M. Cavalca, J. de Oliveira, A. Nied, "Cost function tuning methodology for FCS-MPC applied to PMSM drives", in *2017 Brazilian Power Electronics Conference (COBEP)*, pp. 1–6, IEEE, Juiz de Fora, Nov. 2017, doi:10.1109/COBEP.2017.8257320, URL: <http://ieeexplore.ieee.org/document/8257320/>.
- [16] A. G. Bartsch, D. M. Cavalcanti, M. S. M. Cavalca, A. Nied, "A comparison among different Finite Control Set approaches and Convex Control Set Model-based Predictive Control applied in a Three-Phase Inverter with RL load", in *2019 IEEE 15th Brazilian Power Electronics Conference and 5th IEEE Southern Power Electronics Conference (COBEP/SPEC)*, pp. 1–6, IEEE, Santos, Brazil, Dec. 2019, doi:10.1109/COBEP/SPEC44138.2019.9065706, URL: <https://ieeexplore.ieee.org/document/9065706/>.
- [17] A. G. Bartsch, J. R. Teixeira, J. de Oliveira, M. S. M. Cavalca, "Procedures to Design Multi-Model-Based Predictive Controller Applied to BLDC Drive", *Journal of Control, Automation and Electrical Systems*, vol. 30, no. 6, pp. 994–1006, Dec. 2019, doi:10.1007/s40313-019-00521-7, URL: <http://link.springer.com/10.1007/s40313-019-00521-7>.

- [18] S. F. D. Agnolo, A. G. Bartsch, F. Fernandes, J. De Oliveira, M. S. M. Cavalca, A. Nied, "Convex Control Set Model-Based Predictive Control Applied to a Permanent Magnet Synchronous Motor", in *2023 IEEE 8th Southern Power Electronics Conference and 17th Brazilian Power Electronics Conference (SPEC/COBEP)*, pp. 1–6, Nov. 2023, doi:10.1109/SPEC56436.2023.10407603.
- [19] A. G. Bartsch, *Desenvolvimento de técnicas analíticas de sintonia de controladores preditivos aplicadas ao acionamento de motores síncronos de ímãs permanentes*. Tese de doutorado, Universidade do Estado de Santa Catarina, 2021.
- [20] F. Fernandes, J. d. Oliveira, A. Nied, A. G. Bartsch, "Alternative FCS-MPC concepts for cascade free motor speed control", in *2019 IEEE 15th Brazilian Power Electronics Conference and 5th IEEE Southern Power Electronics Conference (COBEP/SPEC)*, pp. 1–6, IEEE, Santos, Brazil, Dec. 2019, doi:10.1109/COBEP/SPEC44138.2019.9065734, URL: <https://ieeexplore.ieee.org/document/9065734/>.
- [21] A. G. Bartsch, C. J. Meirinho, Y. R. de Novaes, M. S. M. Cavalca, J. de Oliveira, "Analysis of predictive control for boost converter in power factor correction application", in *2016 12th IEEE International Conference on Industry Applications (INDUSCON)*, pp. 1–8, IEEE, Curitiba, PR, Brazil, Nov. 2016, doi:10.1109/INDUSCON.2016.7874470, URL: <http://ieeexplore.ieee.org/document/7874470/>.

BIOGRAPHIES

Arthur G. Bartsch received the BS degree in electrical engineering, and the MS and PhD degrees from State University of Santa Catarina, Joinville, Brazil, in 2015, 2016, and 2021, respectively. Since 2018, he has been an Adjunct Professor with the Department of Electrical Engineering, Federal Institute of Santa Catarina, campus Jaraguá do Sul-Rau, Brazil. His research interests include power electronics, electrical machines, and control theory, focused in predictive control.

Rodrigo Trentini received the BS degree in control and automation engineering from the Instituto Superior Tupy, Joinville, Brazil, the MS degree in electrical engineering from the State University of Santa Catarina, Joinville, Brazil, and the PhD degree in electrical engineering from the University of Hannover, Hannover, Germany, in 2010, 2012, and 2017, respectively. Since 2018, he has been an Adjunct Professor with the Department of Electrical Engineering, Federal Institute of Santa Catarina, campus Jaraguá do Sul-Rau, Brazil. His research interests include power systems modeling and control, renewable energy, control theory, and mechatronics.

Ademir Nied received the BS degree in electrical engineering from the Federal University of Santa Maria, Santa Maria, Brazil, in 1987, the MS

degree in industrial informatics from the Federal Technological University of Parana, Curitiba, Brazil, in 1995, and the PhD degree in electrical engineering from the Federal University of Minas Gerais, Belo Horizonte, Brazil, in 2007. Since 1996, he has been a Faculty Member of Santa Catarina State University, Joinville, Brazil, where he is currently a Full Professor with the Department of Electrical Engineering. From 2015 to 2016, he was a Visiting Professor with the Wisconsin Electric Machines and Power Electronics Consortium, University of Wisconsin- Madison, Madison, WI, USA. His teaching and research interests include electrical machines, control of electrical drives, neural networks, and renewable energy.

José de Oliveira was born in Mandaguari Paraná. He obtained his PhD degree from UFSC in 2000. He is currently a full professor at UDESC. He works in the area of dynamic systems control.

Filipe Fernandes received his BS degree in Electrical Engineering from the Santa Catarina State University (UDESC), where he conducted research in systems control, focusing on predictive control and artificial intelligence applied to power electronics. He is currently pursuing a master's degree in Electrical Engineering at UDESC, with a thesis centered on the development of an Integrated Electric Motor Drive. Filipe works at SUPPLIER, contributing to all stages of the product lifecycle, including design, production coordination, and cost estimation. His experience includes developing AC and DC power supplies, DC-DC and AC-DC converters, and electronic load banks. His main interests are predictive control, motor control, and power electronics.

Sabrina F. dell Agnolo received her BS degree in Electrical Engineering from the Santa Catarina State University (UDESC), where she conducted research in systems control, focusing on predictive control applied to electrical machines. She works at WEG. Her main interests are predictive control, motor control, and power electronics.

Mariana S. M. Cavalca has a BS degree in Control and Automation Engineering from the Federal University of Itajubá (2007) and a PhD in the area of Systems and Control from the Technological Institute of Aeronautics (2011). She holds the position of Associate Professor (with exclusive dedication) at the State University of Santa Catarina (UDESC). She has experience and interest in the area of Control and Automation Engineering, working mainly on the following topics: Predictive Control and Fault Tolerant Control.